Materials Science & Engineering B 225 (2017) 45–53

Contents lists available at ScienceDirect

Materials Science & Engineering B

journal homepage: www.elsevier.com/locate/mseb

Characterization of Ag-doped $Cu_2ZnSnSe_4$ bulks material and their application as thin film semiconductor in solar cells

Albert Daniel Saragih[a], Walelign Wubet[b], Hairus Abdullah[a], Angaw Kelemework Abay[a], Dong-Hau Kuo[a,*]

[a] Department of Materials Science and Engineering, National Taiwan University of Science and Technology, Taipei 10607, Taiwan
[b] Department of Chemistry, University of Gondar, Ethiopia

ABSTRACT

$Cu_2ZnSnSe_4$ (CZTSe) is a promising absorber layer material for thin film solar cells because of the non-toxicity and abundance of the constituent elements. Ag-doped CZTSe bulks and thin films with the $(Cu_{2-x}Ag_x)ZnSnSe_4$ (Ag-*x*-CZTSe) formula at x = 0, 0.1, 0.2, 0.3, and 0.4 were prepared at 600 °C by reactive sintering and selenization. We successfully demonstrated Ag-doped CZTSe materials without any different result between bulks preparation and thin films devices. Defect chemistry was studied by measuring structural and electrical properties of Ag-doped CZTSe as a function of dopant concentration. The enhanced of the device performance are shown with the increasing of Ag content to the CZTSe. The films had a stack structure of Ag/ITO/ZnO/CdS/Ag-CZTSe/Mo/soda-lime glass substrate. The efficiencies of Ag-*x*-CZTSe thin film solar cells at x = 0, 0.1, 0.2, 0.3 and 0.4 were 1.90, 2.4, and 3.4, 3.1, and 2.9%, respectively.

1. Introduction

$Cu_2ZnSnSe_4$ (CZTSe) semiconductor compound has shown the energy conversion efficiencies of 7–11% [1–5], while the highest efficiency reported for the sulfur-selenium alloy CZTSSe has reached 12.6% [6]. CZTSe is a promising absorber layer material for thin film solar cells because of its non-toxicity and abundance of the constituent elements [7]. However, understanding the limitations in this material system is essential for further improvements in device performance. Issues currently observed to limit state-of-the-art CZTSe devices have been the relatively low open-circuit voltage as well as the high reverse saturation currents when compared to high efficiency CIGSe devices [8,9]. One route to improve device performance of CZTSe absorber is through material alloying, where various elements can be incorporated into the tetragonal crystal lattice to modify the optoelectronic properties of the absorber [10]. The natural *p*-type behavior of CZTSe is ascribed to its intrinsic defects and therefore the understanding of such defects can accelerate progress in the solar cell performance. Current knowledge of the electronic properties and especially defect properties is mostly based on theoretical studies carried out using density functional theory [4]. Recently, Ge-incorporated $Cu_2ZnSnSe_4$ (CZTGSe) has demonstrated improved performance for CZTSSe greater than 10% and a high V_{OC} value of 0.54 V [3]. Moreover, the incorporation of stable Ge atoms into the CZTSSe crystal lattice may minimize the formation of deep defects associated with multivalent Sn atoms and is hence beneficial to improve the quality of absorber materials [11]. In order to enhance the property of a certain material for various applications, researchers designed different techniques so as to achieve their interest. So, doping is one of the techniques which have been used to enhance the property of semiconductor materials. Moreover, doping technique helps in studying the defect behavior of semiconductor materials. Here, the investigated Ag doped CZTSe bulks were synthesized by reactive sintering and its thin films and solar cell devices were all demonstrated. Ag is an interesting candidate for the replacement of Cu due to the same chemical group as Cu and a 16% increase in the atomic radius, leading to the intriguing possibility that anti-site defects can be suppressed by increasing the strain required to accommodate each defect [12]. Peter and Boyle had reported that Ag incorporation in the $Cu(In,Ga)Se_2$ (CIGS) alloy system is beneficial for reducing density of extended intragrain defects, defect states and reduced the structure disorder in the absorber since the melting points of Ag-chalcopyrites are 200 °C lower than their Cu analogues [13,14]. Several groups have synthesized of the Ag-alloyed CZTSe thin film solar cells. $(Cu,Ag)_2ZnSnS_4$ thin solar cell was synthesized through sulfurization of Ag/Zn/Cu/Sn metallic stacking layers gave 4.4% efficiency [15], Shao et.al [16] prepared C-AZTSe film via selenization of electrodeposited Cu–Zn–Sn metal precursor with maximum cell efficiency of 7.98%. These efficiencies were shown to be an improvement above the pure CZTSe material; however,

* Corresponding author.
E-mail address: dhkuo@mail.ntust.edu.tw (D.-H. Kuo).

http://dx.doi.org/10.1016/j.mseb.2017.08.007
Received 21 March 2017; Received in revised form 1 August 2017; Accepted 7 August 2017

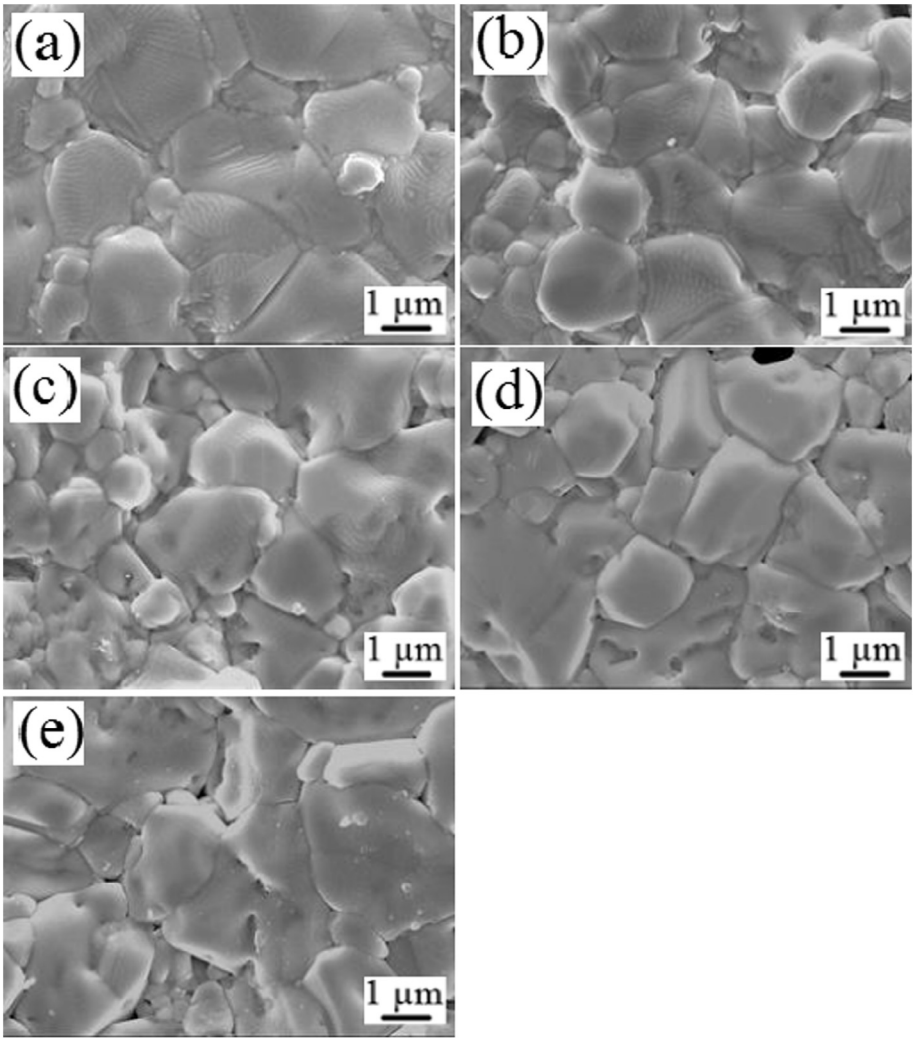

Fig. 1. SEM surface images of $Cu_{2-x}Ag_xZnSnSe_4$ bulks (a) $x = 0$, (b) $x = 0.1$, (c) $x = 0.2$, (d) $x = 0.3$, and (e) $x = 0.4$ after annealing at 600 °C for 2 h.

only few direct measurements have been made to demonstrate how this substitution impacts the fundamental properties of the material.

In this research, we demonstrate the feasibility of the Ag doping in changing the structural compositional characteristics, optical, and electrical properties of CZTSe for better photovoltaic application. We synthesized the $(Cu_{2-x}Ag_x)ZnSnSe_4$ bulks and thin films with atomic Ag-alloy concentrations at the [Ag]/([Ag] + [Cu]) percentages of 0%, 5%, 10%, 15%, and 20%.

2. Experimental

Silver-doped CZTSe material with the formula of $(Cu_{2-x}Ag_x)ZnSnSe_4$ was prepared in the form of bulk pellets with x value of 0, 0.1, 0.2, 0.3, and 0.4 *via* a two-step liquid-phase reactive sintering technique at 600 °C for 2 h with a holding at 300 °C for 1 h. The commercially available ZnSe and self-synthesized binary selenides of Cu_2Se and $SnSe_2$ and the Ag metal powders have been used to prepare Ag-doped CZTSe bulk materials. These constituent powders were separately milled by a planetary ball-milling machine for 6 h to achieve very fine powders and then were mixed by conventional ball milling for 12 h. The liquid-phase reactive sintering technique has been performed by the companion of Sb_2S_3 and tellurium materials which improved the densification of Ag-CZTSe bulks with their lower melting temperatures of 450 °C and 550 °C, respectively. The good densification of the bulks was also necessary for the purpose of electrical measurement. The selenides weighing were based on the actual formula of $[(Cu_{2-x}Ag_x)(Zn_{0.9}Sn_{0.9})Sb_{0.2}](Se_{3.3}S_{0.3}Te_{0.4})$ with x at 0, 0.1, 0.2, 0.3, and 0.4 after considering the compositions of sintering aids. The specimens were symbolized in terms of Ag-x-CZTSe. Ag-x-CZTSe bulks were formed by a cold pressing process at 200 psi. A home-made tube furnace, which was evacuated by a rotary mechanical pump to a base pressure of less than 1 Pa was used for sintering of Ag-x-CZTSe bulks. The $SnSe_2$ disc as a selenium source was placed in the tube and near the bulks for the purpose of providing Se vapor to avoid the Se vaporization from Ag-CZTSe. The tube was filled with pure argon gas at 1 atm during the sintering process.

We prepared metallic target by mixing Cu, Zn, Sn and Ag powders with the formula of $(Cu_{2-x}Ag_x)ZnSn$ with x value of 0, 0.1, 0.2, 0.3, and 0.4 followed by hot pressing. The 2-inch metallic targets were hot pressed at 300 °C under argon with a hydraulic pressure of 400 psi for 30 min. $(Cu_{2-x}Ag_x)$-Zn-Sn precursor thin films were deposited on the Mo/glass substrates by direct-current (DC) magnetron sputtering at 60 W for 1 h. Then the as-deposited films were selenized at 600 °C for 1 h together with a compensation disk containing ($SnSe_2$ + Se) pellet to provide the required Se vapor and convert the metallic into selenide films [17]. The film thicknesses of Ag-doped CZTSe were ~1.2 μm. After the selenization process, the CdS/CZTSe interface was formed by chemical-bath deposition. The 70 nm-thick CdS buffer layer was deposited onto the CZTSe absorber layers via the chemical bath deposition method using a precursor solution consisting of 1.02 M thiourea, 0.84 M ammonia, and 0.18 M cadmium acetate at 70 °C for 15 min [18]. Intrinsic zinc-oxide (*i*-ZnO) and indium-tin-oxide (ITO) window layers were followed subsequently by radio-frequency (RF) sputtering. The ~50 nm ZnO layer was sputtered at 100 °C for 10 min with RF power of 60 W and the ITO 300–350 nm ITO layer was sputtered at

100 °C for 40 min with RF power of 60 W. Finally, the silver paste was used for electrode contact. The thin film solar cells were fabricated with a SLG/Mo/Ag-CZTSe/CdS/ZnO/ITO/Ag configuration is same as to those previously reported [17,19].

The composition and growth morphology of films were characterized using field-emission scanning electron microscopy (FE-SEM, JSM 6500 F, JEOL, Japan) operated with an accelerating voltage of 15 kV and equipped with an energy dispersive spectrometer (EDS). The samples were coated with Pt for 80 s prior to SEM and EDS analyses. Phase identification of the CZTSe layer deposited on soda-lime glass was analyzed by *X-ray* diffraction (XRD, Bruker D2) with Cu-Kα (λ = 1.54056 Å) radiation source operated at 40 kV. *X-ray* photoelectron spectroscopy (XPS) was used to analyzed the element charge state of Ag-doped CZTSe thin films by using VG ESCA with *X-ray* source of Al Kα (1486.6 eV) and argon ion gun operated at 3 kV and 1 mA. Ultraviolet–visible spectrometer (UV–vis-NIR V-670, Jasco) was used to measure the absorption spectra of Ag-doped CZTSe powders. A Hall measurement system (HMS 2000 ECOPIA, Korea) was used to measure the electrical conductivity, mobility, and carrier concentration based upon the van der Pauw method. The illuminated *J–V* characteristic of the device with cell area of 0.16 cm^2 was measured under a standard solar stimulator 1.5 AM illumination at room temperature (100 mW/cm^2).

3. Results and discussion

Fig. 1 shows SEM surface images of $Cu_{2-x}Ag_xZnSnSe_4$ bulks (a) $x = 0$, (b) $x = 0.1$, (c) $x = 0.2$, (d) $x = 0.3$, and (e) $x = 0.4$ after annealing at 600 °C for 2 h. All the bulks had smooth surfaces with clearly defined grain boundaries and they were dense enough to be used for electrical property measurements. Fig. 2 shows SEM surface images of $Cu_{2-x}Ag_xZnSnSe_4$ thin films at (a) $x = 0$, (b) $x = 0.1$, (c) $x = 0.2$, (d) $x = 0.3$, and (e) $x = 0.4$ after selenization at 600 °C for 1 h. All films demonstrate dense packing of the grains with no voids. As a result, the Ag substitution improved the grain growth and densification, here the apparent changes in grain size were observed after the incorporation of dopants into films. The improved grain growth of the Ag substitution in CZTSe up to 20% is one of the advantages for CZTSe being used for solar cell devices. Typically, the enhanced grain growth in CZTSe, as well as CIGSe absorbers, results from an increased liquid phase content in film for liquid-assisted grain growth [10], such as those from Na–Se, Cu–Se, or other liquid phases [20,21]. The large grain in thin films is expected to be beneficial to the short-circuit current of a CZTSe device because the recombination of photo-generated carriers at the grain boundaries can be reduced.

Fig. 3(a) shows EDS composition analyses of $Cu_{2-x}Ag_xZnSnSe_4$ bulks after annealing at 600 °C for 2 h (x = 0–0.4). In order to get more factual data, the corresponding values were recorded by averaging of areal EDS analysis containing at least five different zones on the surface of each sample. The concentrations of Cu, Ag, Zn, Sn, Sb, and total anions (Se, S, and Te) for Ag-*x*-CZTSe bulks after annealing at 600 °C for 2 h are shown in Fig. 3(a). The [Ag]/([Cu] + [Ag] + [Zn] + [Sn] + [Sb]) ratios were 0, 0.025, 0.053, 0.084, and 0.118 and the [Cu]/([Cu] + [Ag] + [Zn] + [Sn] + [Sb]) ratios were 0.498, 0.476, 0.452, 0.429, and 0.396 when the x ratios were 0, 0.1, 0.2, 0.3, and 0.4,respectively. Calculation of these ratios confirms an increase in Ag content and a decrease in Cu content when the x ratios increase from 0 to 0.4. The other constituent elements of the bulks such as Zn, Sn and Sb and the total amount of anions (S, Te, and Se) were almost constant. Sintering the Ag doped CZTSe material at such a low temperature (600 °C) by the help of sintering aids led the atomic composition of the compounds remained as favored and very close to our design formulation. Atomic percentages of total anions Ag-*x*-CZTSe increased from 50.32 to 50.37 as x changed from 0 to 0.4. So, there is no possibility for the formation of Se vacancy in the samples due to the good composition control in the anion site. It is very important to have the anion sites completely occupied by anions of Se, S, and Te, because each of them has the same charge of 2^- and will not create the anion vacancies and the defects with effective charge. On the other hand, it is expected that there are lots of cationic point defects existing in the forms of vacancies, extrinsic defects, and anti-sites for the off-stoichiometric Ag-*x*-CZTSe compounds. Without the mentioned anion problems, the complex defects in Ag-doped CZTSe can be simplified.

Composition analyses of ($Cu_{2-x}Ag_x$)-Zn-Sn films after selenization with ($SnSe_2$ + Se) pellet are shown in Fig. 3(b). The [Ag]/([Ag] + [Cu]) ratios were 0, 0.049, 0.103, 0.153, and 0.205 when the x ratios were 0, 0.1, 0.2, 0.3, and 0.4, respectively, while the [Zn]/[Sn] ratios were 1.157, 1.146, 1.169, 1.195, and 1.18 at those points. The Zn rich compositions in CZTSe have been frequently mentioned for good absorber layers [22,23].

Fig. 4(a) and (b) shows XRD patterns of $Cu_{2-x}Ag_xZnSnSe_4$ bulks after annealing at 600 °C for 2 h and $Cu_{2-x}Ag_xZnSnSe_4$ thin films after selenization at 600 °C for 1 h (x = 0–0.4), respectively. These results were used to confirm the formation of solid solution with negligible second phases. With the confirmations of solid solution and no second phases, the defect consideration can be simplified. The major peaks from (112), (103), (220/204), (312/116), (400/008) and (332/316) were observed for all single phase Ag-*x*-CZTSe thin films and bulks. All the diffraction peaks were attributed from the kesterite structure of pure CZTSe phase, referring to PDF #52 08268 [24]. Fig. 5 shows the magnified XRD plots (112) peaks of (a) $Cu_{2-x}Ag_xZnSnSe_4$ bulks after annealing at 600 °C for 2 h and (b) $Cu_{2-x}Ag_xZnSnSe_4$ thin films after selenization at 600 °C for 1 h (x = 0–0.4). The peak of (112) located at 27.8° and 28.2° for Ag-doped CZTSe bulks and films, respectively. This peak position broadening is due to the crystallite size in direction normal that corresponding of the (hkl) lattice planes. The position of the peak (112) shifted to the lower angel side when the Ag content got increased. Based on the (112) peak shift for Ag-doped CZTSe thin films and bulks, a subsequent calculation of the lattice parameters α and c can be made to study the defect behavior. The lattice spacing of (112) and (220)/(204) peaks were obtained with the help of Diffrac plus EVA software and the lattice parameters were calculated according to the Bragg equation for the tetragonal structure ($a = b \neq c$) [25]. The lattice parameter data can provide an extra evidence for the existence of defects, as seen in Fig. 6. It is found that the lattice parameter α increases from a value of α = 5.526 Å for Ag- free CZTSe (x = 0) to 5.631 Å for Ag-0.4-CZTSe and the lattice parameter c increases from a value of c = 11.054 Å for Ag-free CZTSe (x = 0) to 11.261 Å for Ag-0.4-CZTSe thin bulks. However, in our bulk study of Ag doped CZTSe, large ionic size Te (2.07 Å) and small ionic size S (1.7 Å) were also used as sintering aids. With Sb and Te inclusion, the lattice constants are supposed to increase but on the other hand the inclusion of S in the crystal system has its own contribution to reduce the lattice constants. With this counterbalance effect, therefore, we do not count the effects of Sb, S and Te in lattice parameter. From our EDS analysis, all the total anion contents and the content of Sb^{3+}cation were not deficient at different Cu and Ag contents, their amount is almost constant so their contribution for the defect formation is negligible. And also, Since the Sb^{3+}cation and S^{2-} and Te^{2-} anions have low contents and dissolve into crystal lattice, the defects related to these cation and anions do not need to be considered in the Ag doped CZTSe case. Instead, the Cu and Ag composition differences are accompanied by a variation in cell parameters a and c. For the Ag-doped CZTSe films, the lattice parameter α increases from a value of α = 5.627 Å for Ag- free CZTSe (x = 0) to 5.655 Å for Ag-0.4-CZTSe and the lattice parameter c increases from a value of c = 11.254 Å for Ag- free CZTSe (x = 0) to 11.308 Å for Ag-0.4-CZTSe. The ionic size of Ag^+cation is about 1.15 Å (effective ionic radius, IR), whereas they are 0.77 Å for Cu^+(A^I), 0.74 Å for Zn^{2+}(B^{II}), and 0.69 Å for Sn^{4+}(B^{IV}) in $Cu_2B^{II}B^{IV}Se_4$ [26]. Substitution of Cu^{1+}site (0.77 Å) with big Ag^+ions (1.15 Å), as confirmed by electric property data, can cause the expansion of unit cell. The obvious increases in lattice constants of unit cell indicate that the density of Ag_{Cu} defect

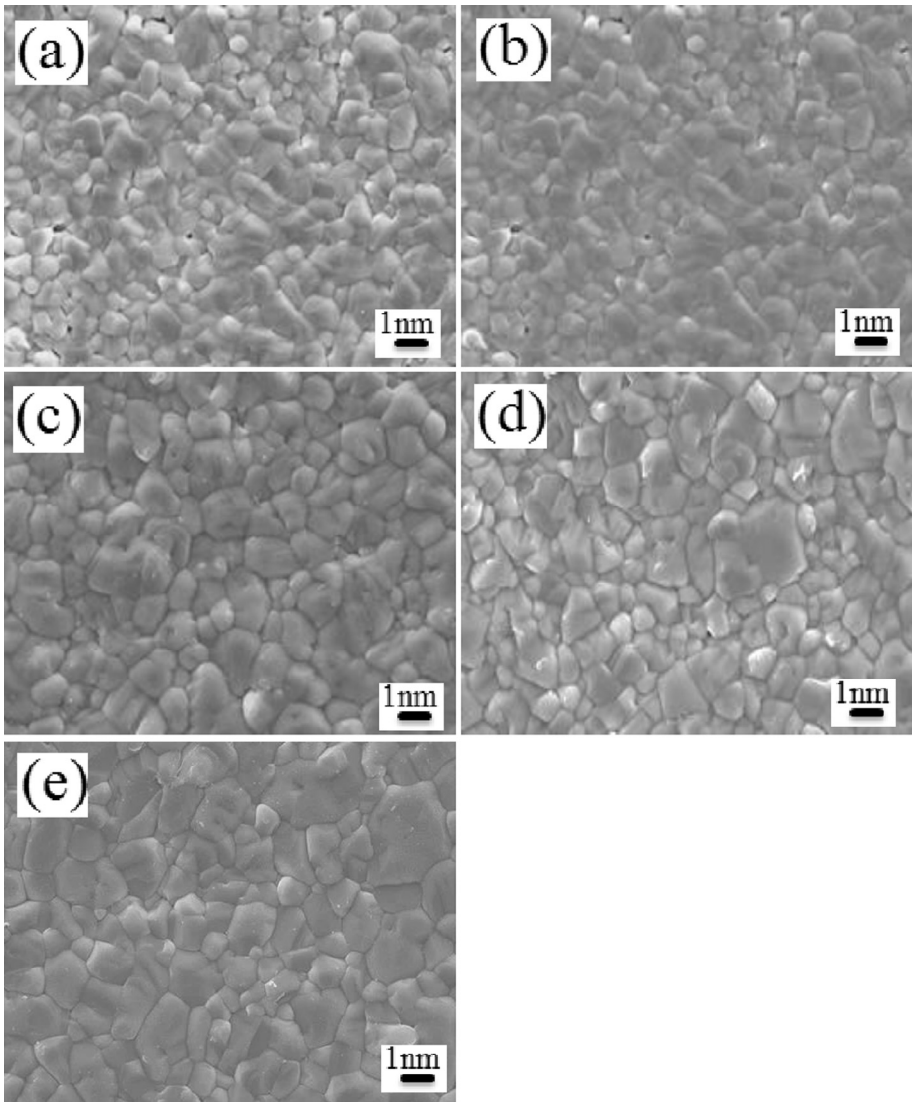

Fig. 2. SEM surface images of $Cu_{2-x}Ag_xZnSnSe_4$ thin films at (a) $x = 0$, (b) $x = 0.1$, (c) $x = 0.2$, (d) $x = 0.3$, and (e) $x = 0.4$ after selenization at 600 °C for 1 h.

becomes much more important in Ag-*x*-CZTSe.

Table 1 shows the carrier concentration, conductivity, and mobility, for Ag-doped CZTSe bulks and thin films at different doping concentrations, respectively. These electrical properties were measured using the van der Pauw method [27]. The Hall voltage (V_H) is measured by forcing both a magnetic field (B) perpendicular to the sample and an input current (I) through the sample. For sample thickness (t) and its resistivity ($\rho = 1/\sigma$), the Hall mobility (μ) can be calculated using

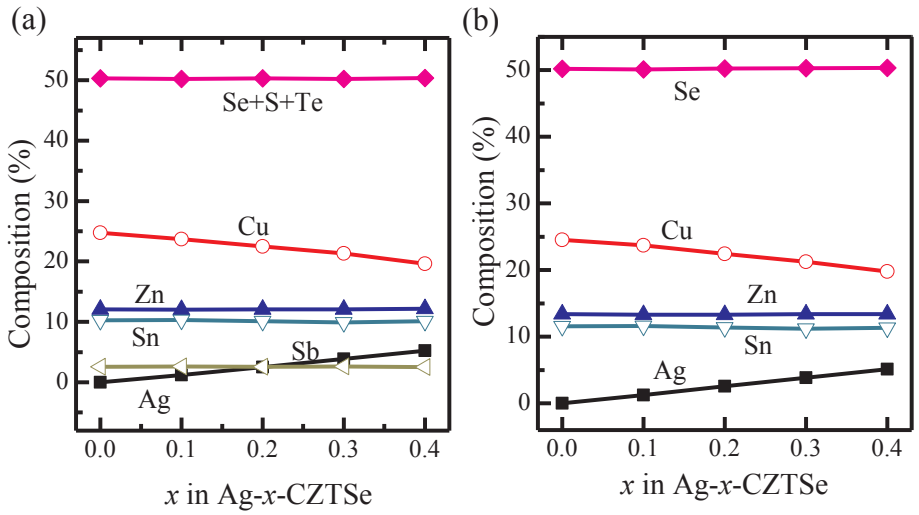

Fig. 3. EDS composition analyses of (a) $Cu_{2-x}Ag_xZnSnSe_4$ bulks after annealing at 600 °C for 2 h and (b) $Cu_{2-x}Ag_xZnSnSe_4$ thin films after selenization at 600 °C for 1 h ($x = 0$–0.4).

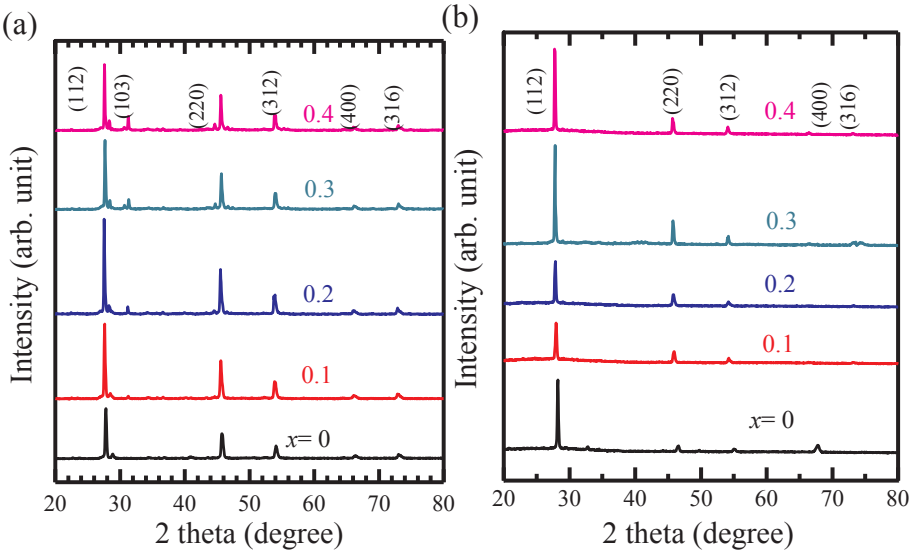

Fig. 4. XRD patterns of (a) $Cu_{2-x}Ag_xZnSnSe_4$ bulks after annealing at 600 °C for 2 h and (b) $Cu_{2-x}Ag_xZnSnSe_4$ thin films after selenization at 600 °C for 1 h (x = 0–0.4).

$\mu = V_H \times t/(B \times I \times \rho)$, and the sheet carrier density of n_e (electron) or n_p (hole) can be calculated via $n = I \times B/(q \times V_H)$ from the known values of I, B, and q, where q is the electric charge. Room-temperature Hall measurements were employed with a magnetic field intensity of 0.51 T and current 0.1 mA. All the Ag-x-CZTSe up to 20% Ag content revealed p-type conductivity, as consistent as those existing reports on Ag-doped CZTSe [12]. The n_p values were 2.17×10^{18}, 1.24×10^{18}, 1.37×10^{17}, 8.12×10^{16} and 9.62×10^{17} cm^{-3} for Ag-x-CZTSe thin films and 3.27×10^{18}, 3.04×10^{18}, 1.07×10^{18}, 8.17×10^{17} and 8.63×10^{17} cm^{-3} for Ag-x-CZTSe bulks at x = 0, 0.1, 0.2, 0.3, and 0.4. Electrical mobility (μ) of Ag-x-CZTSe thin films were 0.47, 0.61, 2.01, 4.65, and 6.59 $cm^2\,V^{-1}\,s^{-1}$ and 20, 20.5, 22, 24.6, and 26.6 $cm^2\,V^{-1}\,s^{-1}$ for Ag-x-CZTSe bulks at x = 0, 0.1, 0.2, 0.3, and 0.4, respectively. The Ag doping in CZTSe leads to high mobility. Electrical conductivity (σ) of Ag-x-CZTSe thin films were 5.1, 6, 7.4, 8.8, and 10.5 $S{\cdot}cm^{-1}$ and 3.2, 4, 4.7, 5.8, and 6.6 $S{\cdot}cm^{-1}$ for Ag-x-CZTSe bulks at x = 0, 0.1, 0.2, 0.3, and 0.4, respectively. The observed trend in carrier concentration is an important electrical property to evaluate for a semiconductor used for solar cell devices. For Cu-poor in pure CZTSe film, the shallow acceptor of copper vacancy (V_{Cu}) and the donor of Zn_{Cu} antisites are the dominant defect, which is responsible for the p-type conductivity. Densities of V_{Cu} defects and Zn_{Cu} antisites are much more in Cu-poor CZTSe materials and the hole concentration decreases with the Cu deficient due to the enhanced the formation of Zn_{Cu} antisites defect [28,29]. As the Zn, Sn, and Se contents were almost constant (Fig. 2b), the defects can be related to the contributions of Ag in CZTSe samples. By doping Ag into CZTSe we were able to reduce the carrier concentration from 10^{18} (for the undoped one) to 10^{16} cm^{-3}. This result indicates that silver dopant preferentially occupies the copper site in CZTSe. As Cu vacancy and defect pairs such as (V_{Cu} + Zn_{Cu}), (Cu_{Zn} + Zn_{Cu}), and (Zn_{Sn} + Sn_{Zn}) are easily formed in the Cu-poor and Zn-rich condition [30], the defect of Ag_{Cu} is also the possible defect. As the x value of Ag increases up to x = 0.3 and always substitutes at the Cu sites, the carrier concentration will expand in a linear way. However, the carrier concentration (Table 2) reach saturated values at higher Ag contents (x > 0.3). This information indicates that the Ag doping in the A site has a concentration limit. In the thin films, the 15% Ag solubility in the Cu site of Ag-x-CZTSe closely reaches the saturation limit and excessive Ag will preferentially occupy the B site to act as an acceptor and to lead to higher carrier concentration at x = 0.4 in Ag-x-CZTSe. To have the Ag-to-B defect behave as an acceptor, Ag can substitute the Zn site or the average B^{2+} site. Due to our design formulation with a Zn-rich, the Ag^{1+}-to-B^{2+} defect will be the dominant defect. Ag^+ has a higher ionic size than Zn^{2+}, therefore the lattice parameters keep enhancing for Ag-x-CZTSe with x = 0.3. Because of the formation of the Ag^+-to-B^{2+} or Ag_B acceptor defect to

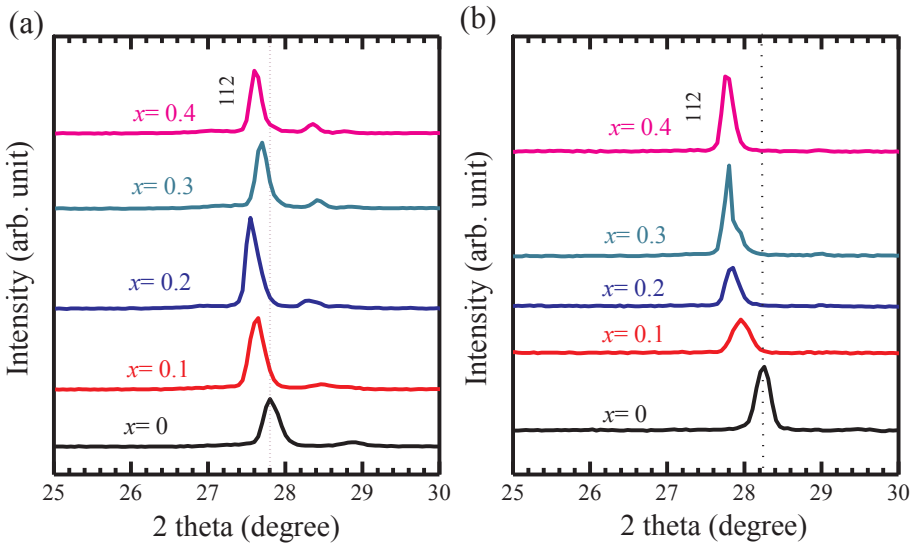

Fig. 5. Magnified XRD of the plots (1 1 2) peaks of (a) $Cu_{2-x}Ag_xZnSnSe_4$ bulks after annealing at 600 °C for 2 h and (b) $Cu_{2-x}Ag_xZnSnSe_4$ thin films after selenization at 600 °C for 1 h (x = 0–0.4).

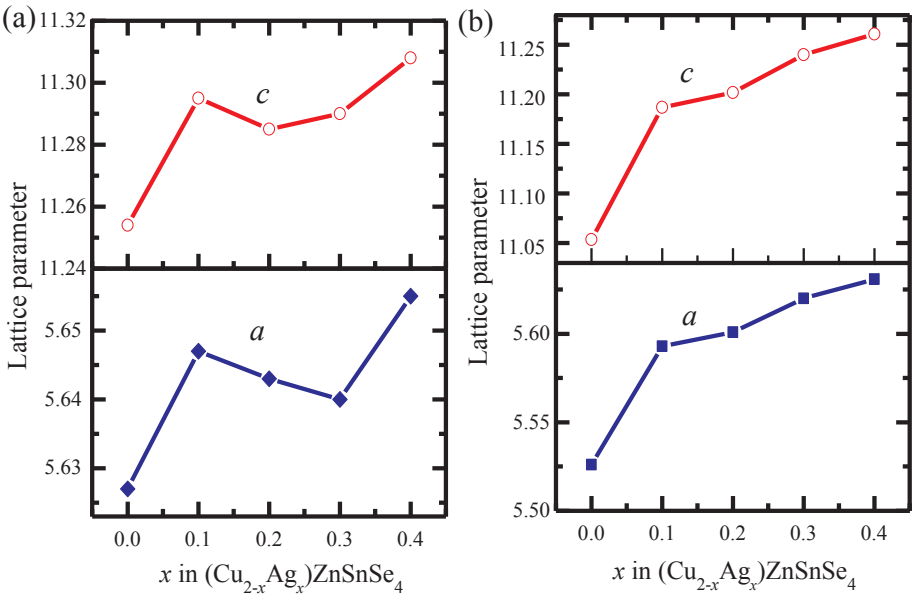

Fig. 6. Lattice parameters (*a* and c) of (a) $Cu_{2-x}Ag_xZnSnSe_4$ bulks after annealing at 600 °C for 2 h and (b) $Cu_{2-x}Ag_xZnSnSe_4$ thin films after selenization at 600 °C for 1 h (x = 0–0.4).

compensate for increasing the carrier concentration. The mobility of semiconductor materials depends on many factors such as crystallinity, grain boundary, atomic scattering, density of carrier concentration, and density of defects. Substitution of zinc ion by silver ion and formation of Ag_{Zn} defects is responsible for increasing the mobility at $x > 0.4$ [12]. For Ag-*x*-CZTSe bulks, the Zn, Sn, and Sb contents and the amount of anions (S, Se, and Te) were almost constant (Fig. 2a). There are no evidences for liquid-phase sintering due to the dissolution of Sb^{3+} into B^{3+} site and the S and Te into Se^{2-} site in the $CuB^{3+}Se_2$ structure after reactive sintering. This could be taken as one of the drawbacks of this preparation method. As the x value of Ag increases up to $x = 0.2$ and always substitutes at the Cu sites, the lattice parameter will expand in a linear way. However, the lattice constant (Fig. 5a) reach saturated values at higher Ag contents ($x > 0.2$). This information indicates that the Ag doping in the *A* site has a limited concentration. In this work, the 15% Ag solubility in the Cu site reaches saturation. Non-stoichiometric $Cu_2ZnSnSe_4$ absorber at the Cu-poor and Zn-rich condition has been used for the solar-to-electrical conversion of solar cell. This $Cu_2ZnSnSe_4$ material does not allow the non-stoichiometry to improve its electrical properties. This is our limitation in bulks preparation, so we propose that point defects generated from the composition deviation are balanced through the ionic compensation for Cu-deficient $Cu_2ZnSnSe_4$ instead of the electrical compensation such as electron and hole. For example, two Cu vacancies are accompanied by two holes in $Cu_2ZnSnSe_4$ but by one S vacancy in $CuSbS_2$ for charge balance. Without the incorporation of acceptor defects, the carrier concentration will drop. Furthermore, the ionic defects behaved as charge-trapping centers to degrade the electrical transport.

XPS analysis was carried out to determine the chemical state of each element in Ag-CZTSe thin films. Fig. 7 shows (a) XPS full scan spectrum of Ag-doped CZTSe thin films and (b) XPS spectra of Cu (2p), Zn (2p), Sn (3d), Se (3d), and Ag (3d) peaks. The binding energy values of Cu $2p_{3/2}$ and Cu $2p_{1/2}$ were 932.30 and 952.10 eV, respectively, with a peak splitting of 19.8 eV are well-consistent with the reported values for Cu^+ [31,32]. Therefore, there is no Cu $2p_{3/2}$ satellite peak located at about 942 eV for the contribution from Cu^{2+}. The chemical state of Zn has been observed from the binding energy of 1022.20 and 1045 eV, which were assigned to Zn $2p_{3/2}$ and Zn $2p_{1/2}$ orbitals, respectively. The standard splitting of 22.8 eV of the Zn 2p peaks suggests Zn in Zn^{2+} state [31]. Tin binding energy values were 486.46 and 495 eV for Sn $3d_{5/2}$ and $3d_{3/2}$, respectively. The Sn 3d peaks with the standard splitting of 8.54 eV suggest it belongs to Sn^{4+} [31]. The binding energy of Se $3d_{5/2}$ peak in the spectrum is 54.9 eV, which is in good agreement with the literature values for Se^{2-} [31]. The binding energy values of Ag $3d_{5/2}$ and Ag $3d_{3/2}$ were 367.71 and 373.69 eV, respectively. Our observed binding energy values of Ag with a peak splitting of 5.98 eV are well-consistent with the reported values for Ag^+ [31].

Fig. 8 shows $(\alpha h\nu)^2$ versus $h\nu$ plots of $Cu_{2-x}Ag_xZnSnSe_4$ bulks (a) $x = 0$, (b) $x = 0.1$, (c) $x = 0.1$, (d) $x = 0.15$, and (e) $x = 0.2$ after annealing at 600 °C for 2 h. The band gap of the bulks was calculated using the Tauc equation. The spectral dependence of the absorption

Table 2
Solar cell performance for devices made of the *p*-type Ag-doped CZTSe with *n*-type layers of CdS/ZnO followed by ITO layer and silver paste for electrode contact.

Modeling	V_{OC}(mV)	J_{SC} (mA/cm^2)	FF (%)	Eff (%)	P_{max} (mW)
$Cu_2ZnSnSe_4$	210	33	27	1.9	0.30
$Cu_{1.9}Ag_{0.1}ZnSnSe_4$	260	36	25	2.4	0.38
$Cu_{1.8}Ag_{0.2}ZnSnSe_4$	298	44	26	3.4	0.55
$Cu_{1.7}Ag_{0.3}ZnSnSe_4$	260	42	29	3.1	0.50
$Cu_{1.6}Ag_{0.4}ZnSnSe_4$	249	41	29	2.9	0.47

Table 1
Electrical properties of bulks and thin films $Cu_{2-x}Ag_xZnSnSe_4$ after selenization at 600 °C (x = 0–0.4).

Modeling	Concentration (1/cm^3)		Mobility (cm^2/V.s)		Conductivity (1/S × cm$^{1)}$	
	Bulks	Films	Bulks	Films	Bulks	Films
$Cu_2ZnSnSe_4$	3.27×10^{18}	2.17×10^{18}	20	0.47	3.2	5.1
$Cu_{1.9}Ag_{0.1}ZnSnSe_4$	3.04×10^{18}	1.24×10^{18}	20.5	0.6	4	6
$Cu_{1.8}Ag_{0.2}ZnSnSe_4$	1.07×10^{18}	1.37×10^{17}	22.01	2.01	4.7	7.4
$Cu_{1.7}Ag_{0.3}ZnSnSe_4$	8.12×10^{17}	8.12×10^{16}	24.65	4.65	5.8	8.8
$Cu_{1.6}Ag_{0.4}ZnSnSe_4$	8.62×10^{17}	9.62×10^{16}	26.59	6.59	6.6	10.5

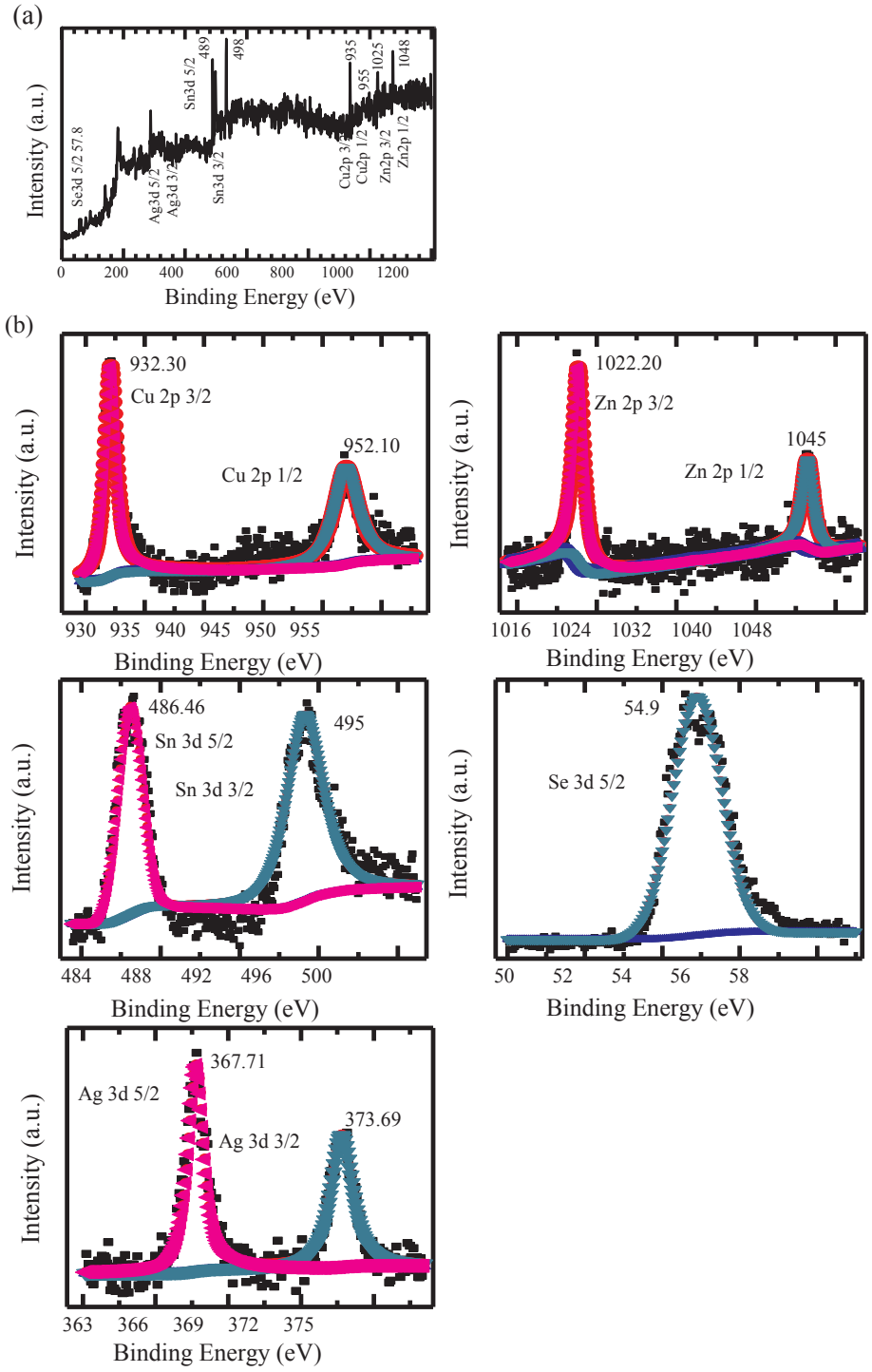

Fig. 7. (a) XPS full scan spectrum of Ag-doped CZTSe thin films and (b) XPS spectra of Cu (2p), Zn (2p), Sn (3 d), Se (3 d), and Ag (3 d) peaks.

coefficient for an allowed direct transition is given by Eq. (1), where α optical absorption coefficient, A a constant, $h\nu$ the incident photon energy, and E_g the energy band gap of the test sample [33].

$$(\alpha h\nu)^2 = A(h\nu - E_g) \quad (1)$$

The band gaps of Ag-x-CZTSe at x = 0, 0.1, 0.2, 0.3 and 0.4 were estimated to be 0.98 eV, 1.07 eV, 1.08 eV, 1.11 and 1.12 eV respectively, by extrapolating the linear region of the plot of $(\alpha h\nu)^2$ versus photon energy ($h\nu$). After increasing Ag content, the band gap shifts to higher values up to ≈1.12 eV for Ag-0.4-CZTSe. The obtained values are consistent with those reported in the literatures that Ag doping can increase the band gap values of CZTSe [10,12,34].

Table 2 shows the cell performance for devices made of the *p*-type Ag-doped CZTSe with *n*-type layers of CdS/ZnO followed by ITO layer and silver paste for electrode contact. The result shows how Ag substitution impacts the device performance by improving the optoelectronic. As shown in Table 2, the open-circuit voltages (V_{OC}), current density (J_{SC}), fill factor (FF), and maximum power (P_{max}) for the pure CZTSe were 210 mV, 33 mA/cm^2, 27%, and 0.3 mW, respectively, while the conversion efficiency (Eff.) was 1.9%. After replacing 5% Cu in CZTSe film with Ag, the device performance showed improvement in the open-circuit voltages (V_{OC}) and the efficiency values up to 260 mV and 2.4%, respectively. Fig. 9(a) show the schematic band diagram of a Ag-10%-CZTSe solar cell under zero-bias voltage condition made of *n*-

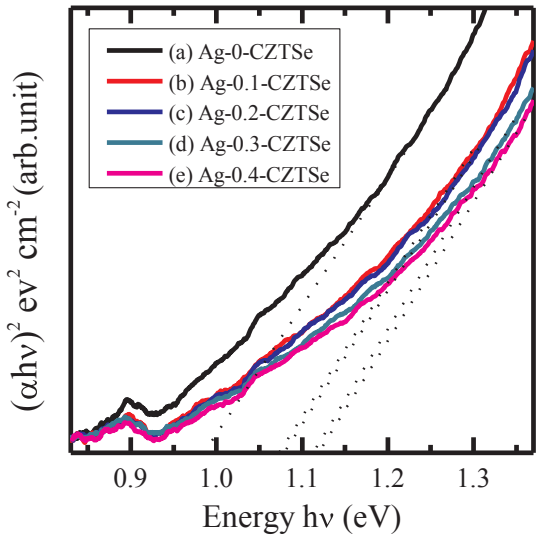

Fig. 8. $(\alpha h\upsilon)^2$ versus hυ plots of $Cu_{2-x}Ag_xZnSnSe_4$ bulks (a) $x = 0$, (b) $x = 0.1$, (c) $x = 0.1$, (d) $x = 0.15$, and (e) $x = 0.2$ after annealing at 600 °C for 2 h.

type CdS/ZnO/ITO under AM 1.5 G simulated illumination. The Mo back contact is covered with a CZTSe absorber layer which optimally has the average band gap energy of 1.08 eV. Fig. 9(b) shows the *J-V* curves of the $Cu_{2-x}Ag_xZnSnSe_4$ thin films solar cell devices (x = 0–0.4). After adding 10% Ag in to CZTSe film, the performance showed the best result in this work. The open-circuit voltages (V_{OC}), current density (J_{SC}), fill factor (FF), and maximum power (P_{max}) were 298 mV, 44 mA/cm^2, 26%, 0.55 mW, and 3.4%, respectively. Cell performance of the 10% Ag on CZTSe thin film solar cells had a 1.5-fold increase. In contrast, 15% and 20% Ag in to CZTSe demonstrates relatively poor device performances. From the data in Table 2, the Ag15% and 20% Ag on CZTSe thin films solar cell showed 3.1% and 2.9% efficiencies with low open-circuit voltages (V_{OC}) of 260 mV and 249 mV, respectively. The open deficit might be due to the morphological properties such as, densification, a flat surface, large grains and electrical properties such as carrier concentration [3].

Device performance for Ag-doped CZTSe reported here is lower than that previously reported for alloyed-kesterite and nanocrystal-based CZTSe absorber [10,12]. However, in this work we reported the effect of Ag dopant to the CZTSe thin films and bulks preparation completed with defect chemistry by measuring structural, electrical and optical properties. Additionally, MgF_2 reflection coating and KCN etching were not utilized for our absorbers reported herein.

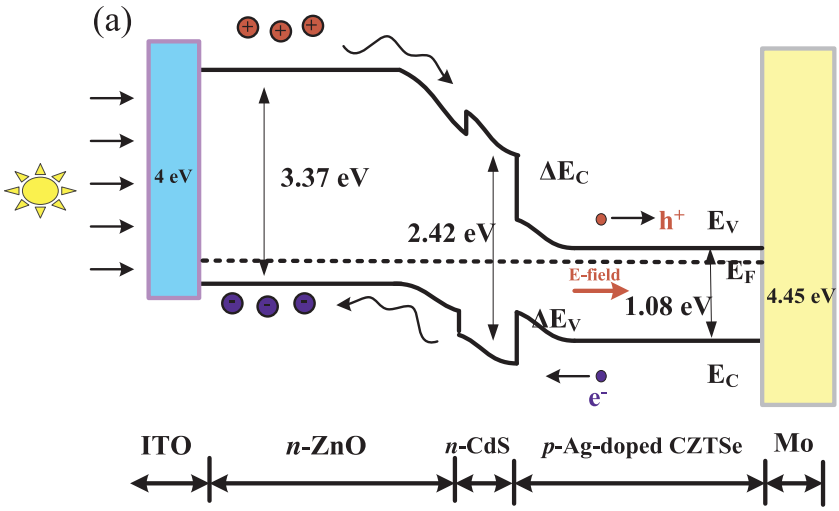

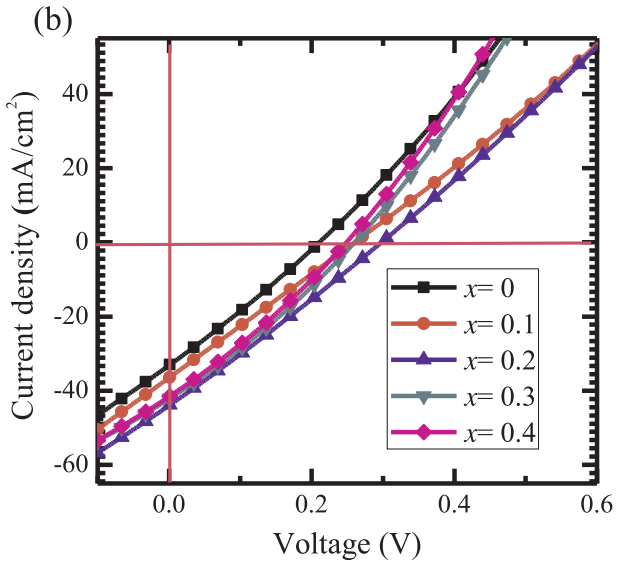

Fig. 9. (a) Schematic band diagram of a Ag-10%-CZTSe solar cell under zero-bias voltage condition made of *n*-type CdS/ZnO/ITO under AM 1.5 G simulated illumination, (b) *J-V* curves of the $Cu_{2-x}Ag_xZnSnSe_4$ thin films solar cell devices (x = 0–0.4).

4. Conclusion

$(Cu_{2-x}Ag_x)ZnSnSe_4$ bulk materials and thin films (x = 0–0.4) were fabricated by reactive sintering and selenization technique at 600 °C. All The Ag substitution improved the grain growth and densification, here the apparent changes in grain size were observed after the incorporation of dopants into CZTSe materials. All Ag-x-CZTSe bulks and films show p-type semiconductor. The direct optical band gaps of Ag-x-CZTSe bulks at x = 0, 0.1, 0.2, 0.3 and 0.4 were estimated to be 0.98, 1.07, 1.08, 1.11 and 1.12 eV, respectively. The enhancements of the device performance are shown with the increasing of Ag content to the CZTSe. Finally, we demonstrated Ag-doped CZTSe thin film solar cells with efficiency 3.4% and V_{OC} value of 298 mV. Cell performance of the 10% Ag on CZTSe thin film solar cells had a 1.5-fold increase.

Acknowledgments

This work was supported by Ministry of Science and Technology of the Republic of China under Grant Nos. 104-2221-E-011-169-MY3 and 104-2623-E-011-003-ET.

References

[1] Y.S. Lee, T. Gershon, O. Gunawan, T.K. Todorov, T. Gokmen, Y. Virgus, S. Guha, Adv. Energy Mater. 5 (2015) 1–4.
[2] S. Oueslati, G. Brammertz, M. Buffière, H. ElAnzeery, O. Touayar, C. Köble, J. Bekaert, M. Meuris, J. Poortmans, Thin Solid Films 582 (2015) 224–228.
[3] S. Kim, K.M. Kim, H. Tampo, H. Shibata, K. Matsubara, S. Niki, Sol. Energy Mater. Sol. Cells 144 (2016) 488–492.
[4] J. Márquez-Prieto, M.V. Yakushev, I. Forbes, J. Krustok, P.R. Edwards, V.D. Zhivulko, O.M. Borodavchenko, A.V. Mudryi, M. Dimitrievska, V. Izquerdo-Roca, N.M. Pearsall, R.W. Martin, Sol. Energy Mater. Sol. Cells 152 (2016) 42–50.
[5] M. Placidi, M. Espindola-Rodriguez, S. Lopez-Marino, Y. Sanchez, S. Giraldo, L. Acebo, M. Neuschitzer, X. Alcobé, A. Pérez-Rodríguez, E. Saucedo, J. Alloy. Compd. 675 (2016) 158–162.
[6] W. Wang, M.T. Winkler, O. Gunawan, T. Gokmen, T.K. Todorov, Y. Zhu, D.B. Mitzi, Adv. Energy Mater. 4 (2014) 1301465.
[7] D.B. Mitzi, O. Gunawan, T.K. Todorov, K. Wang, S. Guha, Sol. Energy Mater. Sol. Cells 95 (2011) 1421–1436.
[8] C.J. Hages, N.J. Carter, R. Agrawal, T. Unold, J. Appl. Phys. 115 (2014) 234504.
[9] J. Lee, W. Lee, N.K. Shrestha, D.Y. Lee, I. Lim, S.H. Kang, Y.-C. Nah, S.-H. Lee, W. Yi, S.-H. Han, Mater. Chem. Phys. 144 (2014) 49–54.
[10] C.J. Hages, M.J. Koeper, R. Agrawal, Sol. Energy Mater. Sol. Cells 145 (2016) 342–348.
[11] D.B. Khadka, S. Kim, J. Kim, RSC Adv. 6 (2016) 37621–37627.
[12] T. Gershon, Y.S. Lee, P. Antunez, R. Mankad, S. Singh, D. Bishop, O. Gunawan, M. Hopstaken, R. Haight, Adv. Energy Mater. 6 (2016) 1502468.
[13] J.H. Boyle, B.E. McCandless, W.N. Shafarman, R.W. Birkmire, J. Appl. Phys. 115 (2014) 223504.
[14] P.T. Erslev, J. Lee, G.M. Hanket, W.N. Shafarman, J.D. Cohen, Thin Solid Films 519 (2011) 7296–7299.
[15] W. Li, X. Liu, H. Cui, S. Huang, X. Hao, 625 (2015) 277-283.
[16] P.W. Shao, C.T. Li, K.C. Ho, K.W. Cheng, J. Power Sources 286 (2015) 47–57.
[17] D.H. Kuo, J.T. Hsu, A.D. Saragih, Mater. Sci. Eng., B 186 (2014) 94–100.
[18] A.C. Lokhande, R.B.V. Chalapathy, J.S. Jang, P.T. Babar, M.G. Gang, C.D. Lokhande, J.H. Kim, Sol. Energy Mater. Sol. Cells 161 (2017) 355–367.
[19] A.D. Saragih, D.-H. Kuo, T.T.A. Tuan, J. Mater. Sci.: Mater. Electron. 28 (2017) 2996–3003.
[20] H. Guo, Y. Cui, Q. Tian, S. Gao, G. Wang, D. Pan, Cryst. Growth Des. 15 (2015) 771–777.
[21] C.M. Sutter-Fella, J.A. Stückelberger, H. Hagendorfer, F. La Mattina, L. Kranz, S. Nishiwaki, A.R. Uhl, Y.E. Romanyuk, A.N. Tiwari, Chem. Mater. 26 (2014) 1420–1425.
[22] H. Katagiri, K. Jimbo, W.S. Maw, K. Oishi, M. Yamazaki, H. Araki, A. Takeuchi, Thin Solid Films 517 (2009) 2455–2460.
[23] T.K. Todorov, K.B. Reuter, D.B. Mitzi, Adv. Mater. 22 (2010) E156–159.
[24] JCPDS (Joint Committee on Powder Diffraction Standards) Card no.00-052-0868.
[25] S.R.S.B.D. Cullity, Elements of X-Ray Diffraction, Prentice-Hall, New Jersey, 2001.
[26] R.D. Shannon, Acta Cryst, A 32 (1976) 751–756.
[27] L.J. Van der Pauw, Philips Res. Rep. (1958).
[28] S. Chen, X.G. Gong, A. Walsh, S.H. Wei, Appl. Phys. Lett. 96 (2010) 021902.
[29] A.R. Jeong, W. Jo, S. Jung, J. Gwak, J.H. Yun, Appl. Phys. Lett. 99 (2011) 082103.
[30] T. Maeda, S. Nakamura, T. Wada, Jpn. J. Appl. Phys. 50 (2011) 04DP07.
[31] W.F.S. John, F. Moulder, Peter E. Sobol, Kenneth D. Bomben, Handbook of X-ray Photoelectron Spectroscopy, Physical Electronic Inc, Minnesota, United States of, America, 1995.
[32] Y.F. Du, J.Q. Fan, W.H. Zhou, Z.J. Zhou, J. Jiao, S.X. Wu, ACS Appl. Mater. Interfaces 4 (2012) 1796–1802.
[33] J.I. Pankove, Optical Processes in Semiconductors, Dover Inc, New York, 1971.
[34] W. Gong, T. Tabata, K. Takei, M. Morihama, T. Maeda, T. Wada, Physica Status Solidi (c) 12 (2015) 700–703.